SCIENTIFIC REPORTS

OPEN

# Multilayer Dye Aggregation at Dye/$TiO_2$ Interface via π…π Stacking and Hydrogen Bond and Its Impact on Solar Cell Performance: A DFT Analysis

Received: 11 August 2016
Accepted: 06 October 2016
Published: 21 October 2016

Lei Zhang[1], Xiaogang Liu[2], Weifeng Rao[3] & Jingfa Li[1]

**Multilayer dye aggregation at the dye/$TiO_2$ interface of dye-sensitized solar cells is probed via first principles calculations, using *p*-methyl red azo dye as an example. Our calculations suggest that the multilayer dye aggregates at the $TiO_2$ surface can be stabilized by π…π stacking and hydrogen bond interactions. Compared with previous two-dimensional monolayer dye/$TiO_2$ model, the multilayer dye aggregation model proposed in this study constructs a three-dimensional multilayer dye/$TiO_2$ interfacial structure, and provides a better agreement between experimental and computational results in dye coverage and dye adsorption energy. In particular, a dimer forms by π…π stacking interactions between two neighboring azo molecules, while one of them chemisorbs on the $TiO_2$ surface; a trimer may form by introducing one additional azo molecule on the dimer through a hydrogen bond between two carboxylic acid groups. Different forms of multilayer dye aggregates, either stabilized by π…π stacking or hydrogen bond, exhibit varied optical absorption spectra and electronic properties. Such variations could have a critical impact on the performance of dye sensitized solar cells.**

Dye sensitized solar cells (DSSCs) utilize molecular dye absorbers to convert photo energy into electrical power[1–4]. The dye/$TiO_2$ interface in the working electrode of a DSSC is responsible for light absorption and charge separation in a DSSC[5,6]. Various researches have been carried out to understand the interfacial dye/$TiO_2$ structures at nanoscale toward formulating structure-property relationship of the photoelectrode and optimizing DSSC performance[7,8].

Substantial first principles calculations have been performed in order to establish an accurate model to describe the nanoscale structures of dye/$TiO_2$ interface[8–11]. Monomeric dye adsorption on $TiO_2$ surface has been extensively evaluated for various dyes to obtain adsorption geometry and dye/$TiO_2$ binding mode[12–14]. Yet, the monomeric dye adsorption model is often inadequate to describe the dye/$TiO_2$ interface; this is due to the fact that many dye molecules are readily adsorbed on the $TiO_2$ surface and form closed packed dye aggregates via intermolecular interactions[15,16]. It has been identified that molecular dye aggregates are responsible for novel optoelectronic properties for functional molecular dyes in DSSCs and related devices, and numerous researches have been performed to manipulate molecular aggregates and fine-tune their materials properties[17–22]. To this end, dimeric dye aggregates at different anchoring positions on the $TiO_2$ surface have been analyzed by Filippo *et al.*[23], offering nanoscopic insights on experimental phenomena that is inconsistent with the monomeric adsorption model. To more closely reassemble experimental scenarios, higher degrees of dye aggregates, such as trimer, tetramer and pentamer, have been constructed via first principles calculations[24]. These aggregation models qualitatively explain the "H-aggregation" phenomena of dyes at the dye/$TiO_2$ interface, where blue-shifted light

[1]Department of Applied Physics, School of Physics and Optoelectronic Engineering, Nanjing University of Information Science and Technology, No. 219 Ning Liu Road, Nanjing 210044, China. [2]Singapore-MIT Alliance for Research and Technology (SMART) Centre, 1 Create Way, 138602, Singapore. [3]Department of Materials Physics, School of Physics and Optoelectronic Engineering, Nanjing University of Information Science and Technology, Nanjing 210044, China. Correspondence and requests for materials should be addressed to L.Z. (email: 002699@nuist.edu.cn)

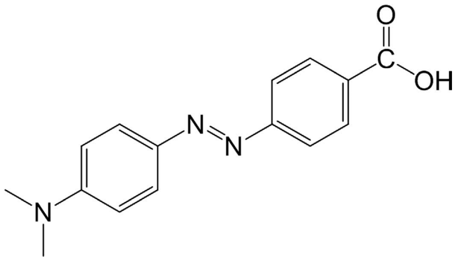


**Figure 1. The molecular structure of 4-[2-[4-(dimethylamino)phenyl]diazenyl]-benzoic acid (*p*-methyl red).**

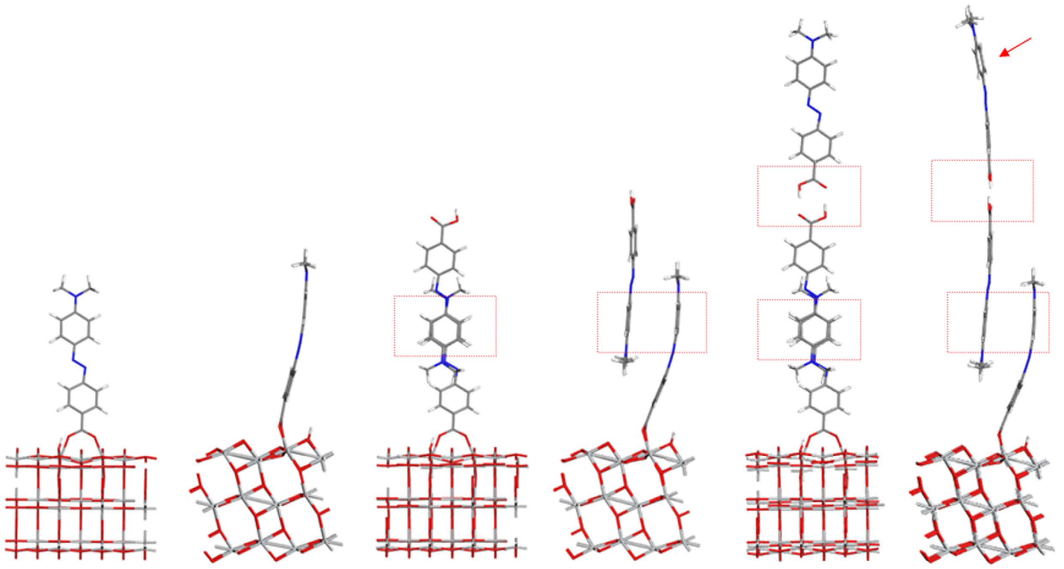


**Figure 2. Optimized geometries of monomer 1, dimer 2 and trimer 3 of methyl red molecules.** Both front view and side view are depicted for clarify. The π…π stacking and hydrogen bond interactions are highlighted in red rectangles. The red arrow points to a potential adsorption site for further aggregate expansion via π…π interaction.

absorption spectra are observed. However, the existing aggregation models are limited in the lateral direction relative to the $TiO_2$ surface, while dye aggregate structures built outward from the $TiO_2$ surface are neglected. In other words, a monolayer model is assumed. The monolayer model sets an intrinsic limitation on the amount of dye adsorption on $TiO_2$ surface, leadings to theoretical predications that are two orders of magnitude smaller than the experimental results[8,24]. An improved multilayer model to describe the interfacial dye aggregates is thus required to bridge the gap between experimental and computational results.

Azo dyes are frequently used in textile and coating industries due to its stability, vivid color, high molar extinction, and low cost[25–27]. Recently, it has been successfully incorporated into DSSCs and convert light into electricity[28,29]. The aggregation of *p*-methyl red azo dyes has been evaluated in previous research in the lateral direction relative to the $TiO_2$ surface[24], and the study on the *p*-methyl red azo dyes serves as a good platform to further analyze their intermolecular interactions and thereby construct the multilayer aggregation model.

In this manuscript, *p*-methyl red [4-[2-[4-(dimethylamino)phenyl]diazenyl]-benzoic acid] is used to probe the dye aggregation on $TiO_2$ surface (Fig. 1). The nanoscale structures of different dye aggregates stabilized via intermolecular forces will be presented, followed by a detailed discussion on their electronic and optical properties that impact solar cell performance.

## Results and Discussion

**Structure of dye adsorbates on a (101) $TiO_2$ surface.** In the optimized structure of the azo dye/$TiO_2$ (Fig. 2), the molecular axis of the adsorbates lies perpendicular to the $TiO_2$ surface. Two molecules in dimer **2** are stabilized by π…π interactions. The top azo molecule in dimer **2** has it carboxylic acid group facing outward away from the $TiO_2$ surface. The separations between two oxygen atoms in the carboxylic acid group and $TiO_2$ surface are similar among **1**–**3** (2.08 Å, 2.07 Å and 2.05 Å for **1**–**3**, respectively), consistent with previously reported values in the literature[24]. The bond lengths of the azo group (-N=N- bond), an indicator of intramolecular charge

| | 1 | 2 | 3 |
|---|---|---|---|
| Adsorption Energy (eV) | 0.60 | 0.43 | 0.56 |
| Dye Coverage (nmol/cm$^2$) | 0.14 | 0.29 | 0.43 |

**Table 1. Estimated adsorption energies and dye coverage levels on the (101) $TiO_2$ surface for different aggregates.**

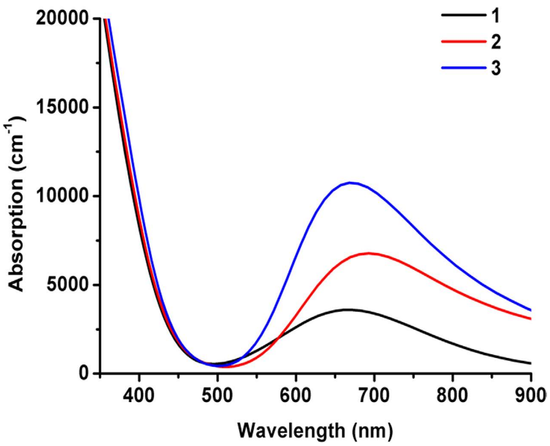


**Figure 3. The calculated UV/vis absorption spectra of 1–3 with *p*-methyl red dye adsorbates on $TiO_2$ substrate predicted by PBE functional.**

transfer[30], are also similar (1.27–1.28 Å) in **1**–**3**. The π…π distance between the two azo molecules are 4.1 Å for both aggregates **2** and **3**, while the H…O distance of the hydrogen bond is 1.53 Å for **3**. Interestingly, the π…π stacking mode and the hydrogen bond interactions between neighboring carboxylic acid groups have been observed in the crystal structures of azo dyes determined from single crystal X-ray diffraction experiment[29]. The monomeric form **1** demonstrates more perpendicular adsorption geometry compared with **2** and **3**. The angle between its molecule axis and $TiO_2$ surface is 3°–4° larger in **1** than that in **2** and **3**. The molecule chemisorbed onto $TiO_2$ surface is more distorted in the case of **2** and **3**, due to steric effects introduced by additional azo molecules.

**Dye adsorption energies and the amount of dye loading on $TiO_2$ surface.** The adsorption energy of the three aggregates follows the ranking: **1** (0.60 eV) >**3** (0.56 eV) >**2** (0.43 eV; Table 1). This is because **1** possesses chemisorption which is more stable in nature than physisorption. **2** is the most unstable system because the intermolecular π…π interaction is based on relatively weak van der waals forces. Molecules in **3** are connected by hydrogen bond which has interaction strength between chemical bonding and van der waals forces.

In terms of dye coverage, **3** has the highest degree of aggregation (0.43 nmol/cm$^2$) among **1**–**3** because it involves three molecules in the unit cell. In contrast, **1** demonstrates the lowest dye coverage (0.14 nmol/cm$^2$). The experimental dye coverage is 147 nmol/cm$^2$ for *p*-methyl red on $TiO_2$ nanoparticles in a DSSC photoelectrode[8]. Although a large discrepancy exists between experimental and calculated values, it is of note that **3** provides adsorption sites for further vertical aggregate expansion (Fig. 2). The outermost molecule in **3** with respect to $TiO_2$ surface can interact with a forth molecule via π…π interactions (indicated by a red arrow in Fig. 2); so on and so forth. In this way, the π…π stacking and hydrogen bond interactions offers a route to construct periodic structures in the *c*-axis, leading to much higher dye loading. As a result, the multilayer aggregation model proposed in this manuscript agrees better with the experimental results[8]. In contrast, the monolayer model in the literature produces a maximum dye coverage of 0.42 nmol/cm$^2$ for *p*-methyl red on $TiO_2$ 2D slab[8], three orders of magnitude smaller than experimental values.

We also noticed that after rinsing dye/$TiO_2$ photoelectrodes during DSSC fabrications (using washing solvent, such as ethanol, to remove weakly adsorbed dye molecules during the sensitization process), the washing solvent displays vivid color due to dye dissolution; this phenomenon indicates that abundant azo dyes are weakly adsorbed on the $TiO_2$ surface such that they can be easily removed from $TiO_2$ substrate. Previous aggregation models, that involve only stable chemisorption, are not sufficient to explain these experimental observations. In contrast, the multilayer aggregation model which incorporates physisorption (such as π…π interaction and hydrogen bond) provides a plausible explanation to the large amount of weakly adsorbed azo dyes on $TiO_2$ substrates.

**Optical Properties.** The calculated UV/vis absorption spectra of **1**–**3** exhibit two major bands: one in the UV region near 400 nm and the other in the visible region from 500 nm to 900 nm (Fig. 3). The intense band in the UV region corresponds to the light absorption in $TiO_2$ substrate, while the visible band corresponds to the absorption of the dye adsorbates. Dimer **2** has the most red-shifted visible band (with peak wavelength at

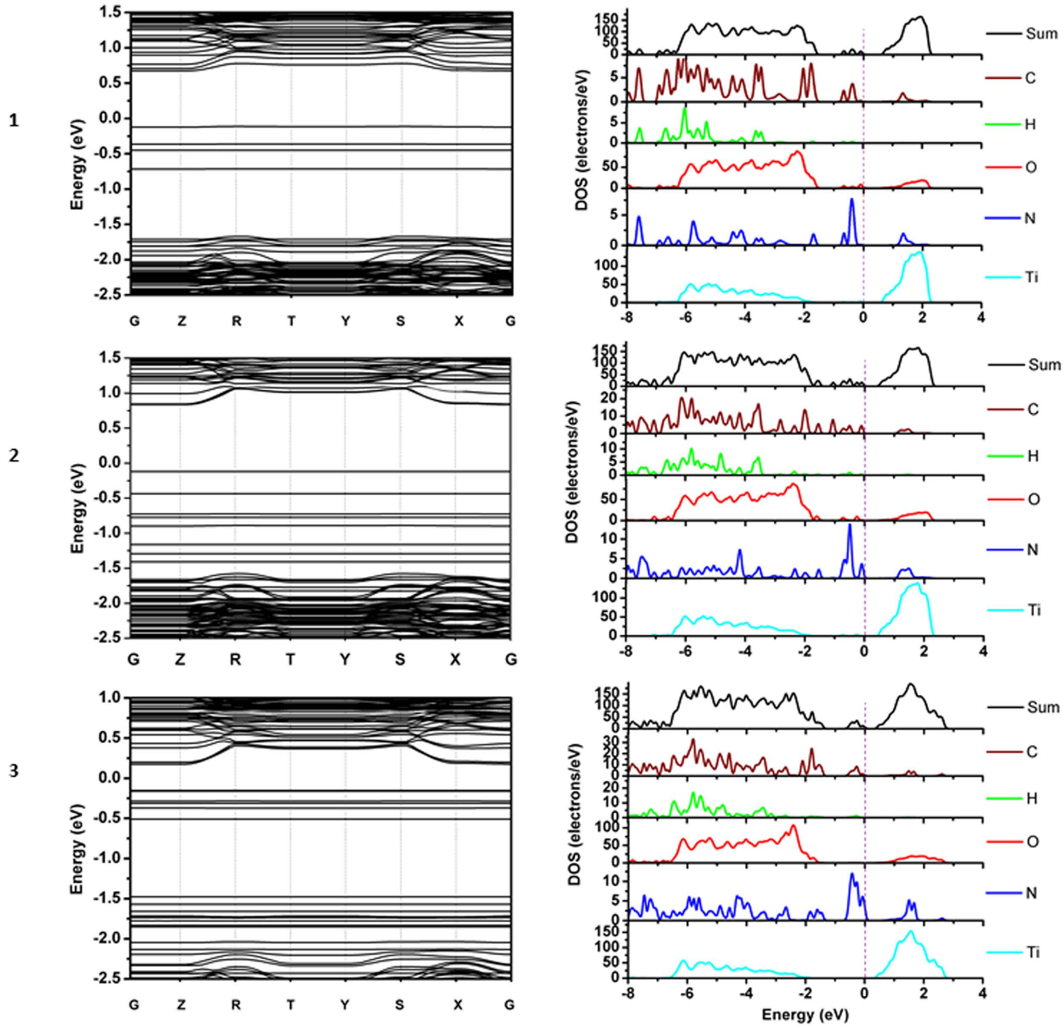


**Figure 4. Band Structures, and projected density of states (PDOS) of C (carbon), H (hydrogen), O (oxygen), N (nitrogen) and Ti (titanium).** The vertical dotted lines correspond to the Fermi Energy, which is set to 0 eV.

693 nm). This peak wavelength is red shifted by 22 nm compared with that of monomer **1**, demonstrating that the π…π stacking interaction is effective in tuning optical properties of DSSC (a red shifted UV/vis absorption spectra is desirable for DSSC device performance for a close match with solar spectrum). Trimer **3** stabilized by hydrogen bond between molecules exhibits the most blue-shifted light absorption spectra among **1–3**, indicating that hydrogen bond between neighboring carboxylic acid anchoring groups in azo dyes is detrimental for improving the light absorption of a DSSC device. The experimental light absorption spectra of the *p*-methyl red/$TiO_2$ film exhibit severe H-aggregation and its peak wavelength approaches the UV region at 400 nm[8]. As a result, the blue-shifted absorption spectrum of **3** implies that the aggregate **3** represents a possible interfacial structure. Further aggregation expansion, which is computationally expensive and unreachable at this stage, is expected to further narrow the gap between experimental and theoretical results. Note that the aggregate **3** does not conform to the typical H-aggregate model, which usually exhibit a head-to-head and tail-to-tail conformation. Instead, the direct "face-to-face" interactions via the hydrogen bonds in aggregate **3** essentially lead to partial dipole-dipole cancellation, because both carboxylic acid groups carry partial negative charge as a result of intramolecular charge transfer in azo dyes[29,31]. The net result of such interactions affords a blue-shift[30,32] in the light absorption spectra of aggregate **3**.

We also notice that the calculated UV/vis spectra of **1–3** (~600 nm) demonstrate a large red shift against experimental data (~400 nm), which has also been experienced in the simulation based on the monolayer model[8]. This is not surprising, because the pure functional PBE (used in our study) neglects Hartree-Fock like exact exchange and tends to severely underestimate the band gap and the excitation energies of charge-transfer dyes (such as azo dyes)[33–35]. Nevertheless, the relative spectral difference among **1**–**3** is more reliable and provides a strong support to our multi-layer aggregation model.

**Band Structure and Density of States.** The band structures of **1**–**3** exhibit a series of straight band lines below Fermi level (Fig. 4). These straight band lines are discrete and are contributed by organic molecules[36]. Nevertheless, these band lines are only defect states and do not affect the electronic band gap of the material.

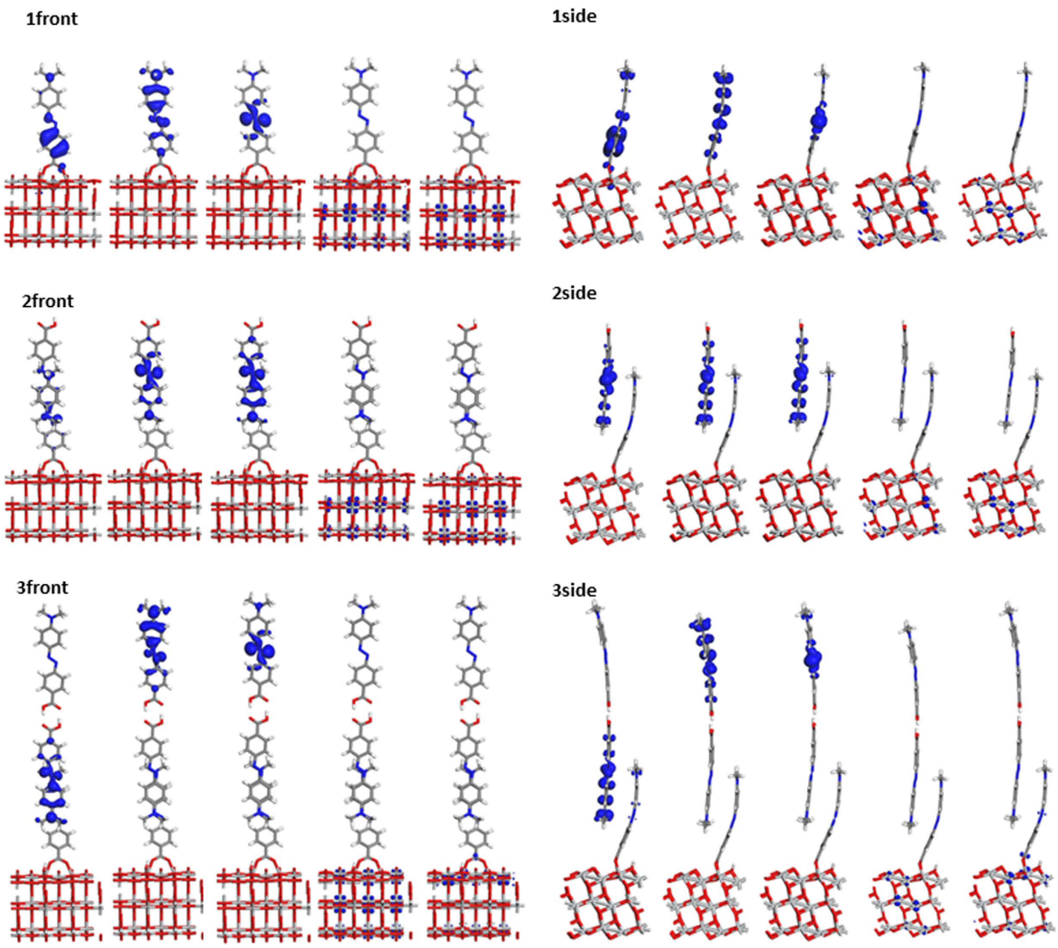


**Figure 5. Orbital distributions of the dye/$TiO_2$ systems.** Five orbitals are presented from left to right of each structure: HOMO-2, HOMO-1, HOMO, LUMO and LUMO+1.

**2** has dense band lines near valence bands contributed by organic dyes. The band lines in **2** are denser than those in **1**, due to more atoms available in **2**. As a result, the optical absorption spectra, which are related to the difference between conduction band and valence band[24], are expected to demonstrate a red-shift in **2** with respect to that in **1**. In the case of **3**, most bands contributed by the chromophore are localized in the deep region between −1.5 and −2.0 eV, which are further away from the conduction band. This could explain the blue shifted absorption spectrum of **3** compared with that of **2**. The band lines with large curvature in the upper and lower regions of the band structure plots are contributed by periodic $TiO_2$ 2D slab.

In the PDOS spectra (Fig. 4), the HOMO (highest occupied molecular orbital) is contributed by carbon, oxygen and nitrogen atoms in the organic molecules. The deep valence bands between −6 eV and −2 eV are mainly contributed by $TiO_2$ oxygen atoms. The conduction band is mainly contributed by Ti atoms in the $TiO_2$ substrate. These features are common in a dye/$TiO_2$ system.

**Orbital Distributions.** The orbital distributions for molecular orbitals HOMO-2, HOMO-1, HOMO, LUMO, and LUMO+1 are depicted to provide an intuitive visualization on the electronic properties of the dye/$TiO_2$ system (Fig. 5). Electron distributions in the unoccupied orbitals are almost the same in **1**–**3**: the LUMO and the LUMO+1 are distributed in the $TiO_2$ region, displaying Ti 3d characters. The occupied molecular orbitals vary among the three structures: for **1**, HOMO is localized in the azo group of the molecule; HOMO-1 is delocalized across the entire azo molecule; HOMO-2 is in the aromatic ring next to the $TiO_2$ surface. In the case of **2**, the HOMO-2, HOMO-1 and HOMO are localized in the upper molecule interacting with the rest of the system via $\pi \ldots \pi$ stacking forces. As a result, this additional molecule in **2** plays an important role in the electronic and optical properties when azo dyes are incorporated in a DSSC device. In the case of **3**, HOMO and HOMO-1 are distributed in the uppermost molecule interacting with the rest system via hydrogen bond, while HOMO-2 resides in the middle molecule. For all the three structures, the outermost molecule is the most active in electronic properties due to HOMO localization in this region, thus having an important impact on the electronic and optical properties of the dye/$TiO_2$ system.

## Conclusions

In this study, we propose a multilayer dye aggregation model to describe the aggregation phenomena in the dye/$TiO_2$ interface. We show that multilayer aggregates may form along the *c*-axis of the dye/$TiO_2$ unit cell via intermolecular interactions, such as π…π stacking and hydrogen bond interactions. Our calculations suggest that further aggregation growth may take place in the *c*-axis, forming a large 3D dye/$TiO_2$ interfacial structure. This multilayer dye aggregation model could thus bridge the gap between theoretical and experimental dye loading on $TiO_2$ surface, in contrast to the monolayer dye adsorption model. Moreover, the weak adsorptions of azo dyes on $TiO_2$ substrate, reported in previous experiments, can be rationalized in the new multilayer model in terms of weak physisorption (in contrast to strong chemisorption in the monolayer model). We also investigated the spectral and electronic properties of the multilayer molecular aggregates as well as their impacts on the DSSC device performance. We show that the π…π stacking induce a red shift, while hydrogen bond leads to a blue shift of the light absorption spectra in the dye/$TiO_2$ system. It is expected that this multilayer model will pave a new way for a deeper understanding of large molecular aggregation systems in DSSC and other relevant applications.

## Methods

A unit cell of $(TiO_2)_{36}$ exposing anatase 101 surface is constructed to analyze the multilayer dye aggregation. A very long vacuum layer and *c*-axis (69.4 Å) of the unit cell is built in order to accommodate the multiple dye molecules in the *c*-axis extending outward from the $TiO_2$ surface. A bidentate bridging anchoring mode for the carboxylic acid anchoring group on anatase 101, suggested by previous research[37,38], is used in this project. Three types of aggregates **1**–**3** are investigated in this study, where **1** represents the monomeric adsorption form; **2** is a dimer joined via π…π stacking effects; **3** is a trimer where a third molecule is placed on top of dimer **2** via hydrogen bond. Upon adsorption, the vacuum layer thickness values are ca. 44 Å for **1**, 39 Å for **2**, and 23 Å for **3**, which are sufficient to minimize interactions between neighbouring layers[39–44]. A $1 \times 3 \times 1$ supercell was constructed to understand the multilayer aggregation, corresponding to a surface area of $10.2 \times 11.3$ Å$^2$. The three interfacial structures **1**, **2** and **3** are geometrically optimized in VASP[45], using PBE functional (energy cutoff: 500 eV; ionic displacement convergence criterion: 0.02 eV/Å). During geometric optimization, oxygen atoms at the bottom of the unit cell are frozen while all other atoms are freely relaxed to their equilibrium positions. The band structures and density of states of **1**–**3** are calculated via an $8 \times 8 \times 1$ monkhorst-pack grid. The optical absorption spectra are obtained from dielectric constant in Castep[46], using 430 eV as the energy cutoff. Graeme D2 dispersion correction[47] is included in all the calculations. The dye adsorption energy on $TiO_2$ surface is calculated using:

$$E_{adsorption} = (n \times E_{dyes} + E_{TiO_2} - E_{dyes/TiO_2})/n$$

The first term in the bracket corresponds to the total energy of molecular dyes; the second is the total energy of bare $TiO_2$ substrate, and the third term is the total energy of the dye/$TiO_2$ system; and *n* is the number of dye adsorbates.

## References


1. O'Regan, B. & Grätzel, M. A low-cost, high-efficiency solar cell based on dye-sensitized colloidal $TiO_2$ films. *Nature* **353,** 737–740 (1991).
2. Kim, S. *et al.* Molecular Engineering of Organic Sensitizers for Solar Cell Applications. *J. Am. Chem. Soc.* **128,** 16701–16707 (2006).
3. Nazeeruddin, M. K. *et al.* Combined experimental and DFT-TDDFT computational study of photoelectrochemical cell ruthenium sensitizers. *J. Am. Chem. Soc.* **127,** 16835–16847 (2005).
4. Hagfeldt, A., Boschloo, G., Sun, L., Kloo, L. & Pettersson, H. Dye-sensitized solar cells. *Chem. Rev.* **110,** 6595–6663 (2010).
5. Law, M., Greene, L. E., Johnson, J. C., Saykally, R. & Yang, P. Nanowire dye-sensitized solar cells. *Nat. Mater.* **4,** 455–459 (2005).
6. Hardin, B. E., Snaith, H. J. & McGehee, M. D. The renaissance of dye-sensitized solar cells. *Nat. Photonics* **6,** 162–169 (2012).
7. Zhang, L. & Cole, J. M. Anchoring Groups for Dye-Sensitized Solar Cells. *ACS Appl. Mater. Interfaces* **7,** 3427–3455 (2015).
8. Zhang, L., Cole, J. M. & Dai, C. Variation in Optoelectronic Properties of Azo Dye-Sensitized $TiO_2$ Semiconductor Interfaces with Different Adsorption Anchors: Carboxylate, Sulfonate, Hydroxyl and Pyridyl Groups. *ACS Appl. Mater. Interfaces* **6,** 7535–7546 (2014).
9. Zhang, L., Cole, J. M., Waddell, P. G., Low, K. S. & Liu, X. Relating Electron Donor and Carboxylic Acid Anchoring Substitution Effects in Azo Dyes to Dye-Sensitized Solar Cell Performance. *ACS Sustain. Chem. Eng.* **1,** 1440–1452 (2013).
10. Ambrosio, F., Martsinovich, N. & Troisi, A. What Is the Best Anchoring Group for a Dye in a Dye-Sensitized Solar Cell? *J. Phys. Chem. Lett.* **3,** 1531–1535 (2012).
11. Hirva, P. & Haukka, M. Effect of different anchoring groups on the adsorption of photoactive compounds on the anatase (101) surface. *Langmuir* **26,** 17075–17081 (2010).
12. Gou, F., Jiang, X., Li, B., Jing, H. & Zhu, Z. Salicylic acid as a tridentate anchoring group for azo-bridged zinc porphyrin in dye-sensitized solar cells. *ACS Appl. Mater. Interfaces* **5,** 12631–12637 (2013).
13. Pastore, M., Mosconi, E. & De Angelis, F. Computational Investigation of Dye–Iodine Interactions in Organic Dye-Sensitized Solar Cells. *J. Phys. Chem. C* **116,** 5965–5973 (2012).
14. Pastore, M. & De Angelis, F. Computational modelling of $TiO_2$ surfaces sensitized by organic dyes with different anchoring groups: adsorption modes, electronic structure and implication for electron injection/recombination. *Phys. Chem. Chem. Phys.* **14,** 920–928 (2012).
15. Pastore, M. & Angelis, F. De. First-Principles Computational Modeling of Fluorescence Resonance Energy Transfer in Co-Sensitized Dye Solar Cells. *J. Phys. Chem. Lett.* **3,** 2146–2153 (2012).
16. Pastore, M. & De Angelis, F. Intermolecular Interactions in Dye-Sensitized Solar Cells: A Computational Modeling Perspective. *J. Phys. Chem. Lett.* **4,** 956–974 (2013).
17. Kim, S. *et al.* H-Aggregation Strategy in the Design of Molecular Semiconductors for Highly Reliable Organic Thin Film Transistors. *Adv. Funct. Mater.* **21,** 1616–1623 (2011).
18. Agrawal, S. *et al.* Modeling the effect of ionic additives on the optical and electronic properties of a dye-sensitized TiO2 heterointerface: absorption, charge injection and aggregation. *J. Mater. Chem. A* **1,** 14675 (2013).
19. Marotta, G. *et al.* An Integrated Experimental and Theoretical Approach to the Spectroscopy of Organic-Dye-Sensitized TiO2 Heterointerfaces: Disentangling the Effects of Aggregation, Solvation, and Surface Protonation. *Chem Phys Chem* **15,** 1116–1125 (2014).

20. Agrawal, S. *et al.* Optical Properties and Aggregation of Phenothiazine-Based Dye-Sensitizers for Solar Cells Applications: A Combined Experimental and Computational Investigation. *J. Phys. Chem. C* **117,** 9613–9622 (2013).
21. El-Zohry, A., Orthaber, A. & Zietz, B. Isomerization and Aggregation of the Solar Cell Dye D149. *J. Phys. Chem. C* **116,** 26144–26153 (2012).
22. Liu, X., Cole, J. M. & Low, K. S. Molecular origins of dye aggregation and complex formation effects in coumarin 343. *J. Phys. Chem. C* **117,** 14723–14730 (2013).
23. Pastore, M. & Angelis, F. De. Aggregation of organic dyes on TiO2 in dye-sensitized solar cells models: an ab initio investigation. *ACS Nano* **4,** 556–562 (2010).
24. Zhang, L. & Cole, J. M. Adsorption Properties of p-Methyl Red Monomeric-to-Pentameric Dye Aggregates on Anatase (101) Titania Surfaces: First-Principles Calculations of Dye/$TiO_2$ Photoanode Interfaces for Dye-Sensitized Solar Cells. *ACS Appl. Mater. Interfaces* **6,** 15760–15766 (2014).
25. Lee, K. M. *et al.* Enhancement of photogenerated mechanical force in azobenzene-functionalized polyimides. *Angew. Chem. Int. Ed. Engl.* **51,** 4117–4121 (2012).
26. Lee, H. Y., Song, X., Park, H., Baik, M.-H. & Lee, D. Torsionally responsive C3-Symmetric azo dyes: azo-hydrazone tautomerism, conformational switching, and application for chemical sensing. *J. Am. Chem. Soc.* **132,** 12133–12144 (2010).
27. Feng, W., Luo, W. & Feng, Y. Photo-responsive carbon nanomaterials functionalized by azobenzene moieties: structures, properties and application. *Nanoscale* **4,** 6118–6134 (2012).
28. Mikroyannidis, J. A., Tsagkournos, D. V., Balraju, P. & Sharma, G. D. Low band gap dyes based on 2-styryl-5-phenylazo-pyrrole: synthesis and application for efficient dye-sensitized solar cells. *J. Power Sources* **196,** 4152–4161 (2011).
29. Zhang, L., Cole, J. M., Waddell, P. G., Low, K. S. & Liu, X. Relating Electron Donor and Carboxylic Acid Anchoring Substitution Effects in Azo Dyes to Dye-Sensitized Solar Cell Performance. *ACS Sustain. Chem. Eng.* **1,** 1440–1452 (2013).
30. Zhang, L., Cole, J. M. & Liu, X. Tuning Solvatochromism of Azo Dyes with Intramolecular Hydrogen Bonding in Solution and on Titanium Dioxide Nanoparticles. *J. Phys. Chem. C* **117,** 26316–26323 (2013).
31. Etter, M. C., MacDonald, J. C. & Bernstein, J. Graph-set analysis of hydrogen-bond patterns in organic crystals. *Acta Crystallogr. Sect. B Struct. Sci.* **46,** 256–262 (1990).
32. Rappoport, D. & Furche, F. Photoinduced Intramolecular Charge Transfer in 4-(Dimethyl)aminobenzonitrile — A Theoretical Perspective. *J. Am. Chem. Soc.* **126,** 1277–1284 (2004).
33. Adamo, C. & Jacquemin, D. The calculations of excited-state properties with Time-Dependent Density Functional Theory. *Chem. Soc. Rev.* **42,** 845–856 (2013).
34. Jacquemin, D., Planchat, A., Adamo, C. & Mennucci, B. TD-DFT Assessment of Functionals for Optical 0–0 Transitions in Solvated Dyes. *J. Chem. Theory Comput.* **8,** 2359–2372 (2012).
35. Perdew, J. P. Density functional theory and the band gap problem. *Int. J. Quantum Chem.* **28,** 497–523 (2009).
36. Liang, J., Zhu, C. & Cao, Z. Electronic and optical properties of the triphenylamine-based organic dye sensitized $TiO_2$ semiconductor: insight from first principles calculations. *Phys. Chem. Chem. Phys.* **15,** 13844–13851 (2013).
37. Gong, X.-Q., Selloni, A. & Vittadini, A. Density functional theory study of formic acid adsorption on anatase $TiO_2$(001): geometries, energetics, and effects of coverage, hydration, and reconstruction. *J. Phys. Chem. B* **110,** 2804–2811 (2006).
38. De Angelis, F., Fantacci, S., Selloni, A., Grätzel, M. & Nazeeruddin, M. K. Influence of the sensitizer adsorption mode on the open-circuit potential of dye-sensitized solar cells. *Nano Lett.* **7,** 3189–3195 (2007).
39. Zhang, S., Yan, Z., Li, Y., Chen, Z. & Zeng, H. Atomically Thin Arsenene and Antimonene: Semimetal-Semiconductor and Indirect-Direct Band-Gap Transitions. *Angew. Chemie Int. Ed.* **54,** 3112–3115 (2015).
40. Zhang, S. *et al.* Semiconducting Group 15 Monolayers: A Broad Range of Band Gaps and High Carrier Mobilities. *Angew. Chemie Int. Ed.* **55,** 1666–1669 (2016).
41. Zhang, S. *et al.* Semiconductor-topological insulator transition of two-dimensional SbAs induced by biaxial tensile strain. *Phys. Rev. B* **93,** 245303 (2016).
42. Zhang, S., Hu, Y., Hu, Z., Cai, B. & Zeng, H. Hydrogenated arsenenes as planar magnet and Dirac material. *Appl. Phys. Lett.* **107,** 022102 (2015).
43. Yu, X., Zhang, S., Zeng, H. & Wang, Q. J. Lateral black phosphorene P–N junctions formed via chemical doping for high performance near-infrared photodetector. *Nano Energy* **25,** 34–41 (2016).
44. Xie, M. *et al.* A promising two-dimensional solar cell donor: Black arsenic–phosphorus monolayer with 1.54 eV direct bandgap and mobility exceeding 14,000 $cm^2V^{-1}s^{-1}$. *Nano Energy* **28,** 433–439 (2016).
45. Kresse, G. & Furthmüller, J. Efficient iterative schemes for ab initio total-energy calculations using a plane-wave basis set. *Phys. Rev. B* **54,** 11169–11186 (1996).
46. Segall, M. D. *et al.* First-principles simulation: ideas, illustrations and the CASTEP code. *J. Phys. Condens. Matter* **14,** 2717–2744 (2002).
47. Grimme, S. Semiempirical GGA-type density functional constructed with a long-range dispersion correction. *J. Comput. Chem.* **27,** 1787–1799 (2006).



## Acknowledgements

This work was supported by the Nanjing University of Information Science and Technology (NUIST) Startup Fund, the Jiangsu Provincial Natural Science Foundation (Grant No. BK20160942 and BK20160941), the Natural Science Fund for Colleges and Universities in Jiangsu Province (Grant No. 16KJB150027 and 16KJB150026), the National Research Foundation of Singapore (through BioSyM Interdisciplinary Research Group at Singapore-MIT Alliance for Research and Technology), the National Research Foundation (NRF), Prime Minister's Office, Singapore, under its CREATE programme, Singapore-MIT Alliance for Research and Technology (SMART) BioSystems and Micromechanics (BioSyM) IRG, the National Natural Science Foundation of China (No. 11474167) and the grant of Specially-Appointed Professor of Jiangsu. The authors acknowledge computational support from NSCC Guangzhou, China and NSCCSZ Shenzhen, China.


## Author Contributions

L.Z. directed the study and performed theoretical calculations. X.L., W.R. and J.L. performed data analysis.

## Additional Information

**Competing financial interests:** The authors declare no competing financial interests.


**How to cite this article**: Zhang, L. *et al.* Multilayer Dye Aggregation at Dye/$TiO_2$ Interface via $\pi\ldots\pi$ Stacking and Hydrogen Bond and Its Impact on Solar Cell Performance: A DFT Analysis. *Sci. Rep.* **6**, 35893; doi: 10.1038/srep35893 (2016).

This work is licensed under a Creative Commons Attribution 4.0 International License. The images or other third party material in this article are included in the article's Creative Commons license, unless indicated otherwise in the credit line; if the material is not included under the Creative Commons license, users will need to obtain permission from the license holder to reproduce the material. To view a copy of this license, visit http://creativecommons.org/licenses/by/4.0/

© The Author(s) 2016